Polymer Chemistry

Accepted Manuscript

This is an *Accepted Manuscript*, which has been through the Royal Society of Chemistry peer review process and has been accepted for publication.

Accepted Manuscripts are published online shortly after acceptance, before technical editing, formatting and proof reading. Using this free service, authors can make their results available to the community, in citable form, before we publish the edited article. We will replace this *Accepted Manuscript* with the edited and formatted *Advance Article* as soon as it is available.

You can find more information about *Accepted Manuscripts* in the Information for Authors.

Please note that technical editing may introduce minor changes to the text and/or graphics, which may alter content. The journal's standard Terms & Conditions and the Ethical guidelines still apply. In no event shall the Royal Society of Chemistry be held responsible for any errors or omissions in this *Accepted Manuscript* or any consequences arising from the use of any information it contains.

ROYAL SOCIETY OF CHEMISTRY

www.rsc.org/polymers

Journal Name

ARTICLE

Towards New Proton Exchange Membrane Materials with Enhanced Performance via RAFT Polymerization

Gökçe Çelik, Murat Barsbay, Olgun Güven†

Received 00th January 20xx,
Accepted 00th January 20xx

DOI: 10.1039/x0xx00000x
www.rsc.org/

This study focuses on the synthesis of well-defined proton exchange membranes (PEM) for fuel cell applications using reversible addition–fragmentation chain transfer (RAFT) polymerization in the radiation-induced grafting part of the overall process. Novel PEMs were prepared via grafting of polystyrene (PS) from poly(ethylene-alt-tetrafluoroethylene) (ETFE) film as a model system. The membranes with various grafting degrees were characterised by ATR-FTIR, Raman, X-ray photoelectron and positron annihilation lifetime spectroscopies, as well as SEM-EDX, AFM, TGA, DSC and DMA techniques. This extensive characterization confirmed the existence of grafted PS chains in copolymer compositions and the success of the subsequent sulfonation. The number-average molecular weight and polydispersity of the non-grafted PS determined by size-exclusion chromatography (SEC) indicated a controlled polymerization in solution. SEM-EDX and AFM results implied that polymerizations were controlled also within the ETFE matrix and on its surface. The introduction of RAFT polymerization in the PEM fuel cell preparation process enhanced the structural uniformity and performance in terms of proton conductivity compared to conventional method.

Introduction

Over the last few decades, there has been a considerable effort in fuel cell materials research for the development of benign energy technologies. Fuel cells are generally considered to be clean and efficient; moreover, they can convert chemical energy to electrical energy at exceptionally high efficiency and without any detectable emissions of pollutants. Among the various types of fuel cells, proton exchange membrane (PEM) fuel cells benefit from high power density, relatively quick start-up, immediate response to changes in power demand and low operating temperatures.[1-3] These properties make them extremely attractive, especially for the transportation sector, which is the main oil consumer in the energy market.[1] Among the PEM fuel cell materials, DuPont's Nafion perfluoro sulfonic acid membrane ranks as the most extensively used membrane material; however, it primarily suffers from dehydration at temperatures exceeding 80 °C and high cost.[3,4]

Conventional radiation-induced grafting (RIG), which relies on generally the grafting of a perfluorinated or partially fluorinated polymer (such as ETFE) with styrene followed by sulfonation, has been widely considered as an effective method for the preparation of alternative PEMs.[5] The versatility of this method lies in its ability to combine a wide variety of base films and monomers to achieve cost-competitive proton exchange membranes. Many efforts have been devoted to the RIG-based preparation of tailor-made PEMs with enhanced properties to replace existing PEM fuel cell membranes with cheaper and ecologically more acceptable materials. To date, this work has been only partially successful. One reason for this may be the absence of control over the molecular weights and polydispersities of grafted polymers, i.e. poorly-defined grafting fashion, which represents a serious shortcoming for conventional RIG. The amount and distribution of proton conducting sulfonic acid groups are among the most critical factors affecting the performance of PEMs.[4] In RIG method, these parameters are directly related with the graft characteristics, e.g. lengths of the grafted chains, their distributions, uniformities, etc. By conventional RIG technique, controlling/tailoring of such properties is not achievable.

In contrast, controlled radical polymerization (CRP) methods efficiently produce well-defined polymers with tailored molecular weights, narrow polydispersities and desired architectures and end-group functionalities.[6] Only three studies have evaluated the incorporation of a CRP method in the RIG step of the PEM preparation process to date.[7-9] Two of these studies[7,8] used the atom transfer radical polymerization (ATRP) technique, whereas the third[9] used the nitroxy-mediated polymerization (NMP) technique. However, none of them discussed the control over grafted or free polymer molecular weights. Furthermore, the studies using ATRP have relied on the primary conventional uncontrolled grafting of a halogen-containing monomer to provide macro-initiators to the substrate for the subsequent ATRP-assisted grafting step.

In this study, we investigated the beneficiary outcomes of performing the PEM synthesis in a fully controlled manner by reversible addition–fragmentation chain transfer (RAFT) polymerization. RAFT polymerization has proven versatile for answering the increasing requirement for highly functional complex polymeric architectures and the global requirements for sustainable chemicals and processes.[10] Furthermore, this technique seems to be a promising synthetic route to prepare well-controlled structures with enhanced performance in specialized applications,[11,12] and it can successfully be combined with RIG.[13-15] The introduction of the RAFT technique in the RIG step in this study does not require substrate functionalization prior to polymerization to control graft growth, which is a significant advantage. Moreover, graft copolymers may lead to more complex structures via further chain

Department of Chemistry, Hacettepe University, 06800, Beytepe, Ankara, Turkey
† guven@hacettepe.edu.tr; www.polymer.hacettepe.edu.tr
Electronic Supplementary Information (ESI) available: [Synthesis Optimizations; Some ATR-FTIR, Raman, XPS, PAL Spectra; Some of the thermal analysis results, GPC chromatograms, AFM and SEM-EDX figures]. See DOI: 10.1039/x0xx00000x

growth or block extension by subsequent monomer addition because of the post-polymerization activity of their chain ends.

Experimental Section

Materials

The 25-µm-thick ETFE base polymer film (Tefzel® 100LZ) was kindly donated from the Paul Scherrer Institute, PSI, Switzerland. Styrene (St, Aldrich, 99%) was deinhibited by percolation through a column packed with activated basic alumina. The chain transfer agent (CTA), cumyl phenyldithioacetate (CPDA), was prepared according to a procedure described elsewhere.[16] Reagent-grade tetrahydrofuran (THF, Aldrich), toluene (Aldrich), methanol (Aldrich), dichloromethane (Merck), chlorosulfonic acid (Riedel-de Haën), NaOH (Fluka), H_2SO_4 (Merck) and HCl (Merck) were used as received.

Grafting

In a typical RAFT-mediated grafting step, desired quantities of St and CPDA were dissolved in toluene. After complete dissolution of the reactants, the stock solution was divided into 15 mL aliquots and transferred to sample glass vials. Then, the ETFE film (ca. 2 cm × 2 cm dimensions, ≈ 0.1 g) was added to the vials as the substrate for grafting. Note that the vials were capped with a rubber septum and deoxygenated by purging with nitrogen gas for 15 min. Then, the samples were placed in a Gammacell 220 ^{60}Co gamma irradiator at ambient temperature at a dose rate of 0.032 kGy h^{-1}. Samples were taken from the irradiator periodically to investigate the reaction kinetics. The monomer conversions were determined gravimetrically after drying the solution in a fume hood followed by a vacuum oven at 30 °C for 3 days. Note that the grafted polystyrene (PS) also contributed to the conversion value. The synthesised ETFE-*g*-polystyrene (ETFE-*g*-PS) films were repeatedly washed with toluene to remove contaminants on the surface. Specifically, each film was placed in a bottle in the presence of toluene (50 mL). The bottles were shaken for up to 2 weeks, and the solvent was changed daily. This process was repeated until no homo-PS was identified in the rinsing solution via SEC analysis after complete evaporation of the solvent. Finally, the ETFE-*g*-PS samples were dried to a constant weight under vacuum at 30 °C. The degree of grafting (DG, wt%) was calculated using:

$$DG = \frac{W_2 - W_1}{W_1} \times 100 \qquad \text{(Eq. 1)}$$

Where W_1 (g) is the weight of pristine ETFE and W_2 (g) is the dry weight of the ETFE-*g*-PS sample. The theoretical number-average molecular weight of homopolymers in solution, M_n^{th}, was calculated according to the following equation:

$$M_n^{th} = M_{CTA} + \frac{n_m^0 \cdot M_M}{n_{CTA}^0} \cdot conversion \qquad \text{(Eq. 2)}$$

where M_n^{th} is the theoretical number-average molecular weight of the polymer, n_m^0 is the initial number of moles of monomer in the system, M_M is the molecular weight of the monomer, n_{CTA}^0 is the initial number of moles of CTA, i.e. CPDA, in the system and M_{CTA} is the molecular weight of the CTA. For comparison, conventional grafting was performed in the absence of CTA. The resulting ETFE films were treated in a manner similar to the samples subjected to RAFT-mediated grafting.

Sulfonation and evaluation of the resulting PEMs

ETFE-*g*-PS films were sulfonated with 10 vol% chlorosulfonic acid in dichloromethane for 2 h at room temperature. They were then hydrolysed in 1 M NaOH solution for 2 h and re-protonated in 1 M H_2SO_4 solution for 3 hours. This process yielded the ETFE-*g*-polystyrene sulfonic acid (ETFE-*g*-PSSA) membranes, which were used as PEMs. Hereafter, the ETFE-*g*-PSSA polymers are designated as membranes while pristine ETFE and PS-grafted ETFE polymers are designated as films.

The ion exchange capacity (IEC) of the resulting ETFE-*g*-PSSA membranes was determined by acid–base titration. The dry weights of the samples were determined after they were dried in a vacuum oven at 60 °C for 24 h. The dried membrane in the protonic form was immersed in 1 M NaCl aqueous solution (20 mL) for 24 h. The solution was then titrated with standard 0.01 M NaOH solution. Based on the titration results, the experimental IEC (meq/g) was calculated as follows:

$$IEC = \frac{M_{NaOH} V_{NaOH}}{W_d} \qquad \text{(Eq. 3)}$$

where M_{NaOH} (M) is the NaOH concentration, V_{NaOH} (mL) is the volume of NaOH solution consumed in the titration and W_d (g) is the dry weight of the PEM in the protonic form. The average IEC value was obtained by repeating the measurements three times for each membrane.

The theoretical IEC was calculated as follows:

$$IEC_{Theor.} = \frac{DG}{M_S + DG \times M_{SSA}} \qquad \text{(Eq. 4)}$$

where M_S and M_{SSA} are the molecular weights of S (104.15 g/mol) and SSA (184.2 g/mol), respectively.

The PEM water uptake was determined by measuring the mass increase due to absorption of water in deionized water at 25 °C for 24 h using the following equation:

$$\text{Water uptake (\%)} = \frac{W_w - W_d}{W_d} \times 100 \qquad \text{(Eq. 5)}$$

where W_w and W_d are the membrane weights in wet and dry states, respectively.

The hydration number (λ), which corresponds to the number of water molecules absorbed per sulfonic acid unit, was calculated from the water uptake and the ion content of the dry membrane according to the following equation:

$$\lambda = \frac{n(H_2O)}{n(SO_3H)} = \frac{\text{water uptake}}{\text{IEC}} \cdot \frac{1}{M_{H_2O}} \qquad \text{(Eq. 6)}$$

where M_{H_2O} is the molecular weight of water (18.01 g/mol).

Before the conductivity measurements, membranes were equilibrated with water vapour for a minimum of 3 days, and then the measurements were performed at 25 °C under nitrogen atmosphere at 95% relative humidity. Proton conductivities were recorded by impedance spectroscopy using the Solartron 1287 Electrochemical interface and the Solartron 1260 Frequency response analyzer. The conductivity (σ) was calculated by the following equation:

$$\sigma = \frac{L}{R \times A} \quad \text{(Eq. 7)}$$

where L is the membrane thickness, R is the resistance and A is the cross-sectional area of the membrane. Membrane bulk conductivity was measured using a BT-112 Conductivity cell designed for in-plane, four-point probe measurements.

Size-exclusion chromatography analysis

Molecular weights of free polymers formed during grafting were analysed at room temperature in THF at a flow rate of 1 mLmin^{-1} using a Waters Gel Permeation Chromatograph equipped with a Waters 515 model HPLC pump. The system was equipped with two Polymer Laboratories 3.0 µm-bead columns (10^5 and 10^3 Å) and a Waters 2414 model refractive index detector. Calibration was performed using PS standards with molecular weights of 200–10^6 g mol^{-1}.

Attenuated total reflectance Fourier transform infrared Spectroscopy (ATR-FTIR)

FTIR spectra were obtained for frequencies ranging from 400 to 4000 cm^{-1} for 64 cumulated scans at 4 cm^{-1} resolution using a Perkin Elmer One FTIR spectrometer. Spectra were recorded in attenuated total reflexion mode using a diamond crystal with single reflection.

Raman spectroscopy

Raman spectra were recorded for frequencies ranging from 50 to 3600 cm^{-1} using a WITec alpha 300 S scanning near-field optical microscope (SNOM) equipped with a Raman module. The light source was a Nd:YAG laser at a wavelength of 532 nm. Data were acquired at a scan speed of 0.1 s per pixel and a diffraction-limited spatial resolution of *ca.* 360 nm. A 100× objective was used to select the area of interest.

X-ray photoelectron spectroscopy (XPS) measurements

XPS measurements were conducted using a Thermo Scientific High-Performance surface analysis instrument equipped with a mono-chromatized Al Kα X-ray source (1486.6 eV photons) at a constant dwelling time of 100 ms for several scans and pass energies of 30 eV for region scan spectra and 150 eV for survey scan spectra. The anode current was set to 20 mA. The pressure in the analysis chamber was maintained at or below 3×10^{-8} mbar during each measurement. ETFE samples were mounted on standard sample studs using double-sided adhesive tape. Core-level signals were obtained at a photoelectron take-off angle of 90° with respect to the sample surface. All binding energies were referenced to the C1s hydrocarbon peak at 285 eV. In peak synthesis, the full width at half-maximum (FWHM) of the Gaussian peaks was maintained constant for all components in a particular spectrum. Surface elemental stoichiometries at ±5% confidence level were calculated from peak area ratios after correction with the experimentally determined sensitivity factors. These elemental sensitivity factors were determined for stable binary compounds of well-established stoichiometries.

Positron annihilation lifetime spectroscopy (PALS)

A ^{22}NaCl droplet from a carrier-free neutral solution (activity: 35 µCi) used as the positron source was dried between two DuPont Kapton® foils (thickness 7 µm), which were subsequently glued together. The source was inserted in 36 identical films in a typical 'sandwich' configuration such that the sample thickness would be sufficient for the annihilation of all the positrons that are formed. PALS experiments were performed using a conventional fast–fast coincidence system exhibiting a time resolution (FWHM) of about 285 ps. Each spectrum was recorded in air at room temperature every 2.5 h for a total count of 1.8×10^6. For each type of sample, 10 spectra were added to produce 1.8×10^7counts. The obtained spectra were analysed using LT program.[17]

Scanning electron microscopy (SEM) imaging and energy dispersive X-ray (EDX) mapping

SEM images were obtained using a FEI Quanta 200 FEG microscope. Sample cross-sections were cut in liquid nitrogen and mounted on a 45°-tilted sample holder for SEM measurements. Supra 35VP Leo EDX instrument was used for sulfur elemental mapping.

Atomic force microscopy (AFM) Analysis

AFM images were acquired in tapping mode in air using a Veeco AFM system equipped with a NanoScope V controller. To investigate the grafting-induced topological changes, pristine ETFE films were hot-pressed between two polished silicon wafers at 5 bar for 5 min at 230 °C prior to grafting. The resultant flat films were then subjected to grafting procedure for AFM investigation.

Thermogravimetric analysis (TGA)

Thermal properties of polymers were recorded using a Perkin-Elmer thermogravimetric analyser (Pyris 1 TGA). Analyses were conducted for temperatures ranging from 25 to 700 °C with a programmed temperature increment of 10 °C min^{-1} under N_2 atmosphere.

Differential scanning calorimetry (DSC)

Temperatures and enthalpies of crystallization and melting were measured using a Netzsch differential scanning calorimeter (DSC 204 F1). Samples were analysed in 25µL pans for temperatures spanning from 20 to 300 °C at a scanning rate of 20 °C min^{-1} under N_2 atmosphere.

Dynamical Mechanical Analysis (DMA)

Storage modulus, loss modulus and tanδ were measured using a dynamical mechanical analyser (TA Instruments Q 800) in tensile mode. A constant amplitude of 20 µm and oscillation frequency of 1 Hz were adopted. Scans were conducted from 30 to 200 °C at 2 °Cmin^{-1} heating rate.

Results and discussion

Synthesis of PS-grafted ETFE films via RAFT polymerization

RAFT polymerization is one of the most versatile methods that provides living characteristics to radical polymerization. A living RAFT polymerization hinges on CTAs or RAFT agents, which are capable of reversibly deactivating propagating radicals such that the majority of living chains remain in a dormant state, and reaction conditions, which support a rapid equilibrium between active and

dormant chains.[18] Therefore, appropriate RAFT agent and reaction conditions are crucial for a successful polymerization. CPDA has previously been found suitable for the γ-initiated RAFT polymerization of styrene; therefore, it was employed in this study.[13] In addition to affecting the RAFT process, reaction conditions, such as monomer and RAFT agent concentrations and absorbed radiation dose, dictate the observed DG values. The effects of monomer concentration at different reaction times and absorbed radiation dose on the DG values of the synthesised films are shown in Figures S1 and S2, respectively (Electronic Supplementary Information). The grafting ratio increased steadily with styrene (St) concentration up to ca. 30% St before rising further at a lower rate (Fig. S1). Therefore, the optimum St concentration was determined as 30% for the rest of the study. Similarly, the DG increased quickly with absorbed dose between 0.5 and 2 kGy before slowing down and becoming almost constant beyond *ca.*10 kGy (Fig. S2). Full molecular weight distributions obtained at 30% (v/v) St and various polymerization times are shown in Fig. S3 for the free PS formed during graft polymerizations. These polymers exhibited narrow and unimodal molecular weight distributions (Fig. S3) regardless of monomer and RAFT agent concentrations (Fig. S4 and Fig. S5). Moreover, the number-average molecular weight, M_n, evolved linearly with conversion (Fig. S6) for homopolymers formed in solution. These results clearly indicate that the grafting process occurs in a controlled manner under various reaction conditions.

The molecular weight (M_n) linearly increased with conversion, suggesting that CPDA provides a good control over the polymerization and leads to low polydispersity (PD) homopolymers, which show molecular weights close to those expected (Table 1). Increasing the RAFT agent concentration relative to that of the monomer reduced homopolymer molecular weights and resulted in narrower PDs at comparable conversions, indicating that polymerizations in solution occurs via the RAFT mechanism (entries 2, 7–9, Table 1).[13,14] However, conventional RIG provided significantly higher M_ns and broader PDs (control, Table 1; Fig. S7).

Polymers such as ETFE can reportedly be grafted by radiation along their whole cross-section, although they scarcely swell in solvents. Grafting in such systems proceeds via grafting front mechanism, in which the initial grafting occurs on the uppermost surface layers, creating a front that may swell well in grafting medium.[19-21] Then, monomers diffuse through this grafted layer and undergo grafting in the subsequent layer. For our system, ETFE does not swell either in toluene or styrene. But, PS grafted ETFE layers swell well in styrene/toluene solution, enabling the diffusion of monomer and RAFT agents inwards. When a substrate is irradiated, radicals are formed both on the surface and inside the matrix due to the high penetration of gamma radiation. Therefore, the diffused monomer molecules meet the radicals in bulk and are grafted to the inner layers via the RAFT mechanism. This process continues by generating new fronts and enriching them until fronts from both sides of the ETFE film meet. Thus, the whole cross-section is grafted; otherwise proton conductivity between the anode and the cathode cannot be attained.

In general, three different groups of PS chains form in such a grafting medium: free homopolymers in solution, surface grafted PS chains (surface grafts) and chains grafted within the ETFE film (inside grafts). It has been demonstrated previously that the propagation of the surface grafted chains is in a dynamic equilibrium with homopolymers in solution and free and surface grafted polymers present almost the same characteristics in a γ-initiated RAFT-mediated grafting.[13] However, the propagation of the inside grafts is expected to differ fundamentally from that of free polymers formed in solution and chains grafted to the uppermost surface.

A polymer swollen in a solvent acts as a high-viscosity medium and the viscosity of the grafted layers plays an important role in monomer diffusion towards grafting sites in a front-mediated grafting process.[21,22] Therefore, the propagation of the inside grafts strongly depends on monomer transport rates and concentrations.[21] Furthermore, each grafted ETFE layer may reflect differences in PS graft enrichment stemming from variations in amorphous and crystalline region amounts because grafting is expected to occur primarily in amorphous or amorphous/crystalline interfacial regions.[23] The polymerization kinetics in solution and on the uppermost surface is expected to differ significantly from that within the ETFE bulk primarily because monomer and RAFT agents present different availability. Moreover, the viscous ETFE filament matrix may restrict the mobility of inside grafts, which leads to a decrease in termination by mutual recombination. Although the control of termination has been of primary focus in the development of RAFT process, the specificity and efficiency of initiation, re-initiation and chain equilibration/propagation steps equally need to be regulated.[24] The ability of the RAFT process to control the molecular weights of the inside grafts cannot be simply accounted for experimentally because the cleavage and segregation of the covalently grafted PS chains, i.e. inside and surface grafts, are unlikely. However, SEM-EDX and AFM analyses revealed that CPDA diffuse into ETFE and mediate a controlled grafting of St within the matrix via RAFT mechanism (please see below), regardless of the differences between ETFE bulk and solution.

Table 1. Number-average molecular weight (M_n) and polydispersity (PD) values for free polystyrene (PS) formed during γ-initiated graft polymerization of styrene (St) from ETFE mediated via the RAFT agent cumyl phenyldithioacetate (CPDA)[a]

entry	dose / kGy	[St] / [CPDA]	convn[b] / %	DG[b] / wt%	M_n^{th}[c] / g·mol^{-1}	$M_{n,SEC}$[d] / g mol^{-1}	PD[d]
1	1.4	700	2.9	56	2400	1620	1.15
2	2.4	700	3.9	70	3125	2170	1.13
3	3.7	700	6.8	76	5230	3140	1.14
4	5.3	700	10.7	77	8070	5590	1.15
5	8.3	700	16.1	90	12000	9420	1.18
6	11.5	700	21.2	95	15730	11260	1.22
7	3.1	350	3.9	61	1700	1110	1.07
8	3.1	1050	5.2	69	5990	4100	1.16
9	3.1	1400	5.8	71	8770	5030	1.17
control[e]	3.1	-	8.4	75	-	37250	2.23
control[e]	7.7	-	16.1	104	-	40160	1.81

[a] Reversible addition–fragmentation chain transfer (RAFT) polymerization of St (2.62 mol L^{-1}) from ETFE (ca. 0.02 g) initiated via γ-irradiation (dose rate: 0.032 kGy·h^{-1}) in toluene at [St]:[CPDA] = 700:1 and room temperature. [b] Monomer conversion and degree of grafting (DG) determined gravimetrically. [c]Theoretical number-average molecular weight (M_n^{th}) calculated from the monomer conversion using Eq. (2). [d]Number-average molecular weight (M_n) and polydispersity (PD) determined via size-exclusion chromatography (SEC) using tetrahydrofuran (THF) as eluent with polystyrene (PS) standards for free PS formed during the graft polymerization of St from ETFE.[e] Conventional grafting of St (2.62 mol L^{-1}) from ETFE initiated via γ-irradiation.

Fig. 1 shows the SEM micrograph of the entire cross-section of ETFE-*g*-PS film with 26% DG and its corresponding EDX dot map, illustrating the distribution of sulfur atoms across the image. In the EDX map, bright red dots highlight high sulfur concentration areas. Sulfur atoms were detected though the entire cross-section (Fig. 1b) because of the RAFT chain-end moieties of the inside PS grafts. This result is very significant because it clearly demonstrates that PS grafts grow within the ETFE matrix via RAFT mechanism. Moreover, the distribution of the sulfur atoms indicates homogeneous grafting across the cross-section. After sulfonation of this sample, the detected sulfur atom amount increases significantly as can be seen in Fig. S8. The uniform distribution of sulfur atoms proves that both the grafting and subsequent sulfonation occur homogeneously.

The surface topography of pristine ETFE as measured by AFM was not uniform at the nano- to micro-scale (Fig. S9). To investigate the grafting-induced topological changes, ETFE films were first hot-pressed between two polished silicon wafers prior to grafting, which drastically reduces the surface roughness (Ra) to ca. 3 nm (Fig. 2a). Conventional and RAFT-mediated grafting significantly increased the surface roughness of these flat ETFE substrates (Fig. 2b-2f). However, RAFT-mediated grafting (Fig. 2b-2d) yielded prominently more homogeneous topography compared to conventional grafting (Fig. 2e and 2f). This may originate from the narrow polydispersity, controlled synthesis and homogeneous distribution of the grafted chains.[19] In addition to these observations by AFM, the grafted films synthesized via RAFT also appeared homogeneous for lower and higher graft levels, which is not always achievable by conventional grafting. This also indicates that RAFT mediates homogeneous grafting on and within the film in a controlled manner.

Characterization of PS-grafted ETFE films and sulfonated membranes

The structures of pristine ETFE, PS-grafted ETFE at 50% DG and the corresponding sulfonated membrane were studied by FTIR spectroscopy (Fig. S10). Spectra showed characteristic peaks of PS in the 2700–3200 cm^{-1} region for PS-grafted ETFE and the sulfonated membrane, demonstrating the grafting of PS. Bands were also detected at 3002, 3027, 3059, 3082 and 3104 cm^{-1}, consistent with the C–H stretching of the phenyl CH groups of the

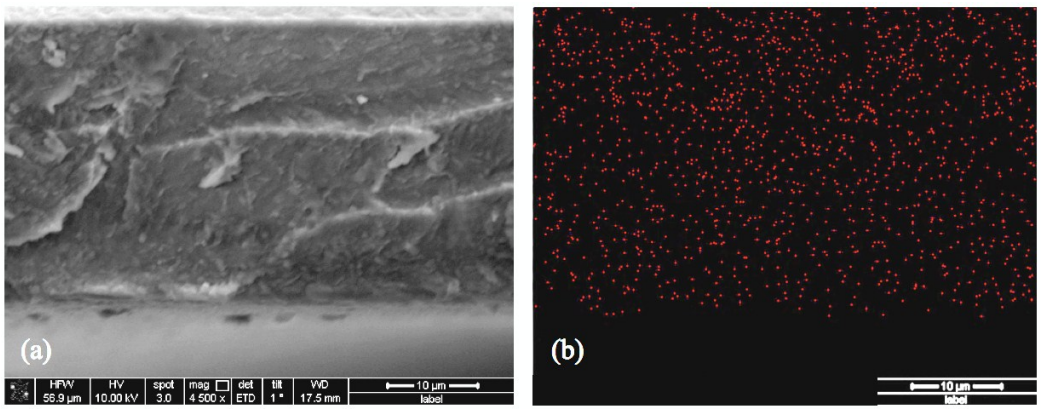

Fig. 1. SEM (a) and corresponding SEM-EDX dot mapping illustrating the distribution of sulfur atoms (b) across the cross-section of ETFE-*g*-PS, DG: 26%

PS side chain. Moreover, bands corresponding to the C–H stretching vibrations of the CH and CH_2 groups in main chain PS were located at 2855 and 2925 cm^{-1}, respectively.[25] Aromatic C=C stretching vibrations of phenyl rings appear at 1494 and 1601 cm^{-1}. Bands were observed at 696 and 756 cm^{-1}, which were attributed to the out-of-plane ring and hydrogen deformations of the mono substituted phenyl groups, respectively.[26] Because of the introduction of sulfonic acid groups into the grafted films, a broad peak appeared at 3000–3600 cm^{-1} region due to the absorption of water molecules by the $–SO_3^-H^+$ groups. The spectrum showed abroad band at 1600–1700 cm^{-1}, which correspond to the sulfonic acid–OH groups. Peaks centred at 1004 and 1135 cm^{-1} were ascribed to the vibrations of sulfonate-substituted phenyl rings.[27] The sulfonated membrane showed a peak at 832 cm^{-1}, which was assigned to the C–H out-of-plane vibration in para-disubstituted benzene.[28,29] This observation indicates that sulfonation occurs at the para position on the benzene ring.

The grafting of PS to ETFE was further evaluated by Raman spectroscopy. Pristine ETFE exhibited two intense bands at about 832 and 2975cm^{-1} (Fig. 3a), which were attributed to CF_2 and CH_2 stretching, respectively.[30] The spectrum of ETFE-*g*-PS at 54% DG (Fig. 3b) clearly differed from that of ETFE and contained characteristic Raman bands for pure PS (Fig. S11), confirming the grafting of PS to ETFE. A strong peak corresponding to the ring-breathing vibrations of phenyl units was detected at 1004 cm^{-1} (Fig. 3b). A peak observed at 1608 cm^{-1} was attributed to aromatic C=C stretching vibrations.[31] Bands at 2855 and 2906 cm^{-1} were assigned to aliphatic C–H stretching, whereas a peak detected at 3054 cm^{-1} corresponded to aromatic C–H stretching vibration.[32] A peak was expected at *ca.* 780 cm^{-1} as a result of the RAFT chain-end groups of the grafted PS. However, this C–S stretching vibration was not detected because the high-intensity absorption bands of ETFE and PS saturated this region.

XPS has proven powerful for the detailed analysis of surface chemical composition. The elemental surface compositions of pristine ETFE, PS-grafted films with various DG values and their corresponding sulfonated membranes were calculated from the XPS wide-scan survey spectra (Fig. S12). These results are summarised in Table 2. ETFE is an equimolar copolymer that mostly consists of a highly alternated structure. Ideally, its structure may be described as a regular alternate sequence of ethylene and tetrafluoroethylene monomers $(CH_2CH_2CF_2CF_2)_x$. Although the C1s/F1s ratio was expected to be 1.00 for pure ETFE, the calculated value from XPS amounted to 0.82. Commonly observed in commercial ETFE samples, this discrepancy was attributed to the non-equimolar monomer composition.[33] As shown in Table 2, the C1s/F1s ratio expectedly increased with DG because of the incorporation of carbon-rich PS units. A significant F atom contribution was observed for all samples, even at the highest DG. This shows that the XPS-detectable top surface layers (ca. 5 nm) are not composed of only pure PS, further indicating that grafting proceeds via front mechanism rather than simple surface grafting. Remarkably, XPS detected sulfur (S) atoms in PS-grafted samples at 20% and 26% DG, suggesting the presence of the RAFT PS chain-end groups and proving that grafting occurs via RAFT mechanism. Significant S and O atom contributions were observed in sulfonated membranes, consistent with a successful sulfonation reaction. The F atom fractions in ETFE-*g*-PSSA membranes were significantly lower compared to their precursor PS grafted films (Table 2), showing that membrane surfaces became enriched with grafts upon sulfonation of PS. This reveals a significant reorientation of the grafts after the sulfonation step as a result of interactions between sulfonic acid units.

To further assess the changes in sample surface composition, XPS C1s emission lines were analysed in detail. The C 1s spectrum of the pristine ETFE film was curved-fitted with two peak components presenting binding energy (BE) values of 286.6 and 291.3 eV for the CH_2 and CF_2 species, respectively (Fig. 4a).[11] Figures 4b and 4d show the C 1s core-level spectra of ETFE-*g*-PS films with 26% and 50% DG, respectively, whereas Figures 4c and 4e show those for their corresponding sulfonated membranes. All spectra exhibited components with BE values of ca. 286.0 and 290.5 eV corresponding to CH_2 and CF_2 species, respectively (Fig. 4b–e), which were assigned to the ETFE main chains. A new peak appeared at a BE value of ca. 284 eV in the C 1s spectra of PS-grafted films (Fig. 4b and Fig. 4d) and sulfonated membranes (Fig. 4c and Fig. 4e). This contribution was attributed to aliphatic CH and aromatic C=C species in grafts and the relative area of this peak increased proportionally with DG. The area of this peak was remarkably higher for sulfonated membranes compared to their PS-grafted precursors, further indicating the occurrence of PS chain reorientations upon sulfonation.

Table 2. X-Ray photoelectron spectroscopy (XPS) elemental composition results of pristine and graft-type ETFE samples.

Sample	F (%)	C (%)	O (%)	S (%)	C/F
ETFE	54.5	44,5	-	-	0.82
ETFE-*g*-PS, DG: 20%	47.6	51.9	0.2	0.2	1.09
ETFE-*g*-PS, DG: 26%	44.7	54.7	0.46	0.14	1.22
ETFE-*g*-PS, DG: 50%	33.1	66.9	-	-	2.02
ETFE-*g*-PSSA, DG: 26%	25.9	56.6	13.6	3.9	2.19
ETFE-*g*-PSSA, DG: 50%	16.6	61.4	15.7	6.3	3.70

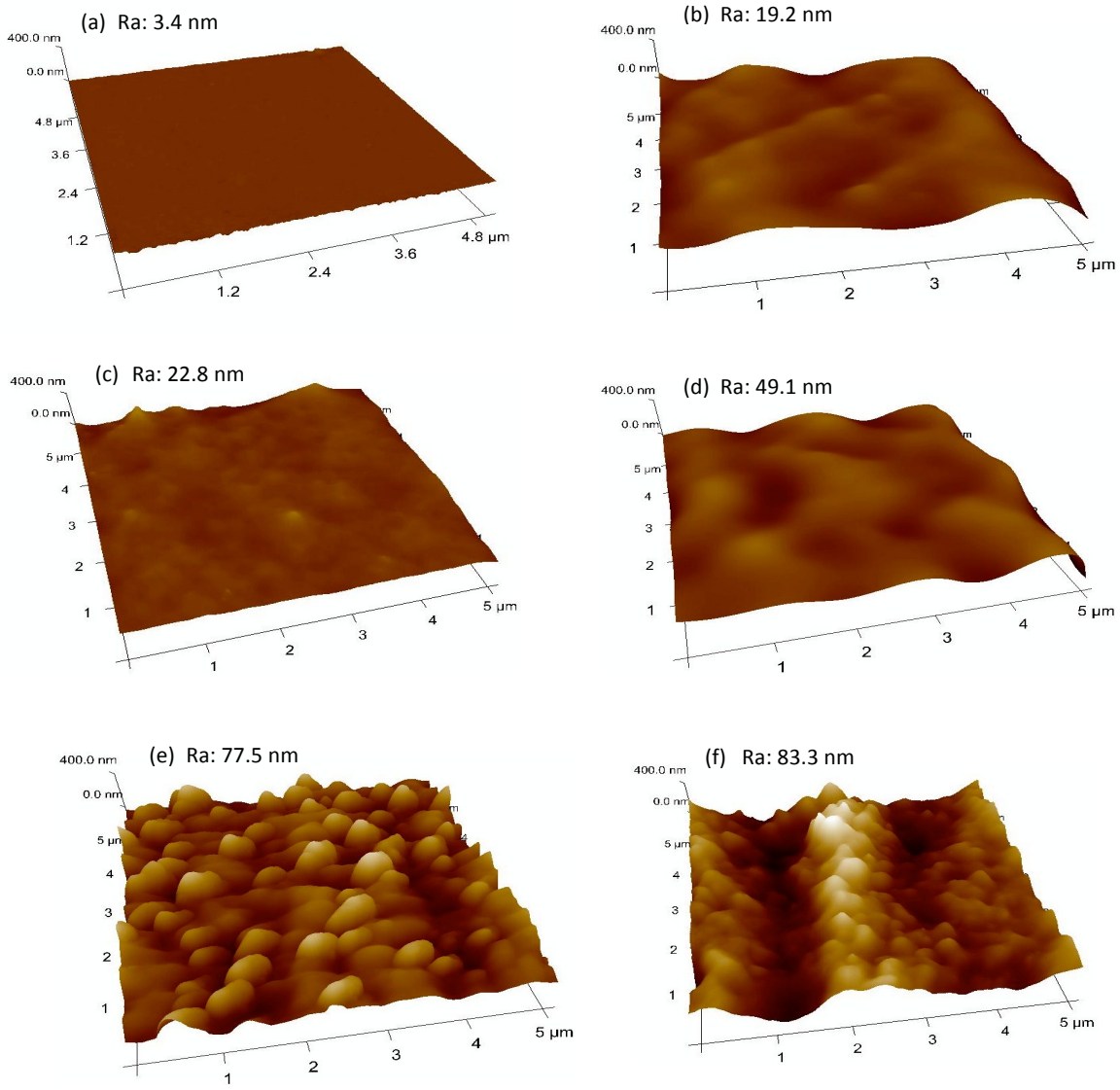

Fig. 2. AFM images and roughness (Ra) values: hot-pressed non-grafted ETFE film (a), RAFT-mediated grafted films with degree of grafting of 15% (b), 20% (c), 37% (d) and conventional (non-RAFT) grafted films with degree of grafting of 25% (e), 37% (f). Hot-pressed ETFE film was used for the preparation of the grafted films.

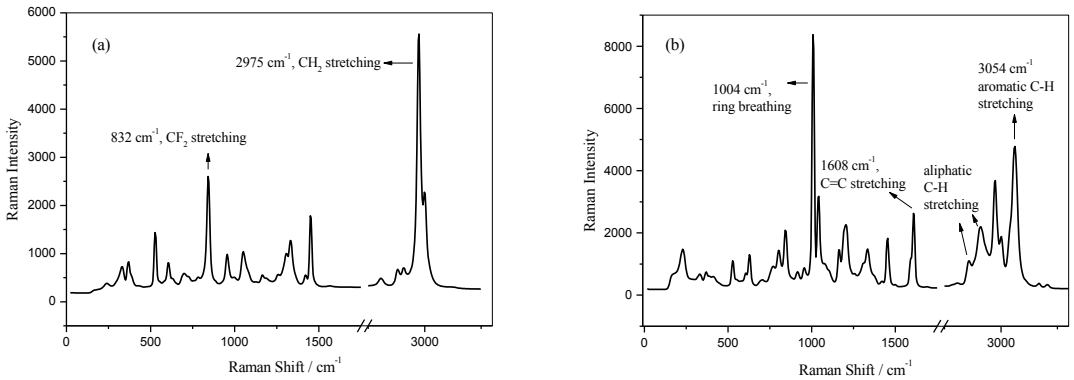

Fig. 3 Raman spectra of (a) pristine ETFE film, (b) ETFE-*g*-PS film with 54% degree of grafting, DG.

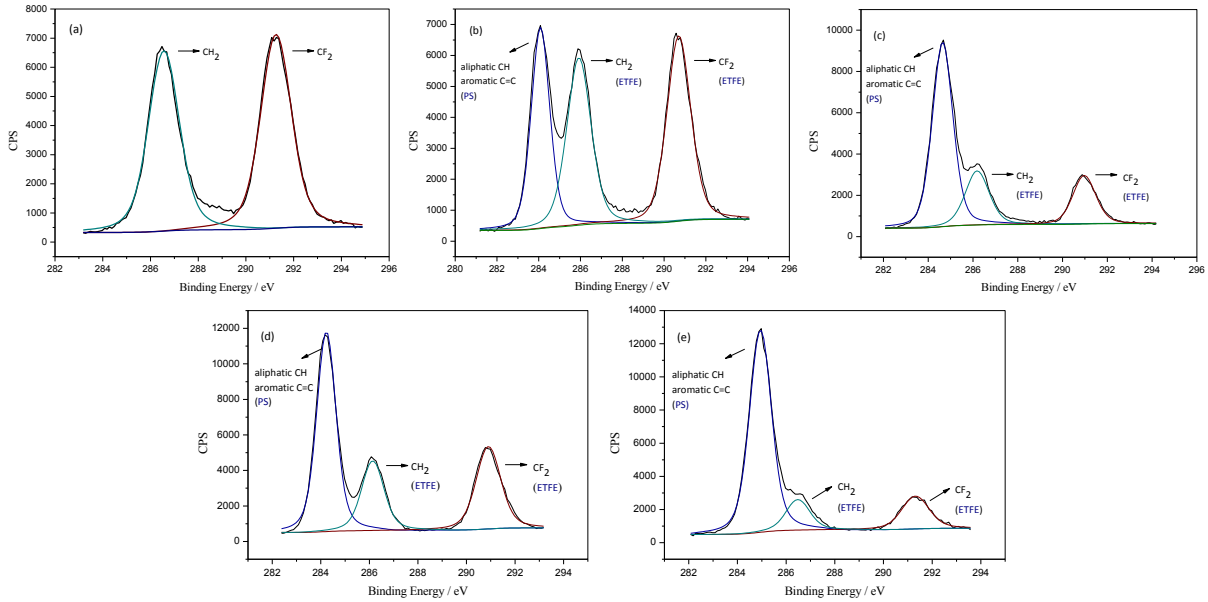

Fig. 4 C 1s spectrum and its components for (a) pristine ETFE, (b) ETFE-*g*-PS film with 26% degree of grafting (DG) and (c) its sulfonated membrane, (d) ETFE-*g*-PS film with 50% degree of grafting (DG) and (e) its sulfonated membrane

In addition to enabling proton conduction, PEM fuel cell membranes serve as a barrier between anode and cathode reactants and an electronic insulator. If hydrogen and oxygen permeate through the membrane, they are consumed to generate heat and water without providing the desired work, leading to fuel inefficiency.[34] Furthermore, oxygen permeation through the membrane may lead to the formation of peroxide and hydroperoxide radicals in the membrane, potentially causing membrane degradation and reducing PEM life-span.[35] In general, gas diffusion in a polymer film is associated with nanometer-sized free-volume holes.[36] Therefore, the amount and size of these holes through the membrane cross-sectional area should be considered to develop advanced PEM materials with low gas crossover.

PAL spectroscopy can uniquely probe nanometer-sized free-volume holes. This technique is sensitive to all isolated and interconnected free-volume pores for sizes ranging from 0.3 to ca. 30 nm and it has been employed to determine pore sizes and their relation to oxygen permeability in polymer membranes.[37,38] Positrons (e^+) possess high kinetic energies when they are created. When a high-energy positron collides with solid matter, it loses energy through inelastic processes such as ionization and electronic excitation, and eventually reaches thermal equilibrium with this solid before diffusing into it.[39-41] During this diffusion process, the positron interacts with the defects in the solid, trapping of the particle in localized states. The positron exists in these defects or free-volume holes, for a short period of time before annihilation.[39-41] This annihilation occurs in the free state or through formation of a bound state with an electron, which is called as a positronium atom, and is often denoted by the symbol Ps. Positroniums exist in two different states (*para*- and *ortho*-), and they differ greatly in mean lifetime (τ). O*rtho*-positronium (o-Ps) exhibits the longest τ value and its lifetime correlates strongly with the size of the free-volume holes according to a quantum mechanical model developed by Tao[42] and Eldrup et al..[43]

A PAL spectrum is generated from a few million annihilation measurements and can typically be deconvoluted into four components with lifetimes τ_i and intensities I_i (Fig. S13). The four detected components were numbered from 1 to 4 starting with the shortest lifetime and ending with the longest one. Components 1 and 2 were attributed to the lifetimes of *para*-Ps and free positron, respectively, while components 3 and 4 were assigned to *ortho*-Ps in different regions, i.e. crystalline and amorphous. In crystalline domains, polymer chains are regularly and densely packed with small intermolecular free-volume holes. In contrast, polymer chains adopt a random configuration in amorphous regions, yielding larger free-volume voids between chains. Therefore, the lifetimes of short- (τ_3) and long-lived o-Ps(τ_4) were attributed to crystalline and amorphous regions, respectively.[44,45] Table 3 lists the measured o-Ps lifetimes (τ_3 and τ_4) and the radius of free-volume holes (R) for crystalline (R_3) and amorphous regions (R_4) calculated using the Tao–Eldrup equation given in ESI.[42,43] Moreover, the intensities (I_2, I_3, and I_4) of PAL spectrum components are compared in Table 3 Because the o-Ps lifetime correlates with the size of free-volume holes, it decreases when the holes shrink. A comparison of τ_3 and τ_4 values measured for pristine ETFE with those published for Nafion and PTFE reveals that crystalline and amorphous regions show significantly lower lifetimes and thus smaller holes, suggesting that ETFE is a better option in terms of gas permeability.[38]

Table 3. Results of PAL measurements of pristine and graft-type ETFE samples.

Sample	τ_3 (ns)	τ_4 (ns) (amorf)	R_3 (nm)	R_4 (nm)	I_2	I_3	I_4
ETFE	0.00217 ±0.004	2.518 ±0.020	-	0.328 ±0.002	46	9.6	12.6
ETFE-*g*-PS, DG: 17%	0.790 ±0.005	2.433 ±0.030	0.126 ±0.001	0.321 ±0.001	44	11.4	23.3
ETFE-*g*-PS, DG: 38%	1.027 ±0.007	2.359 ±0.010	0.170 ±0.001	0.315 ±0.001	34.7	18.6	23.5
ETFE-*g*-PS, DG: 53%	0.284 ±0.002	2.291 ±0.010	-	0310 ±0.001	31	26.7	30.4
ETFE-*g*-PSSA, DG: 15%	0.634 ±0.002	2.354 ±0.020	0.087 ±0.001	0.315 ±0.002	50.6	12.7	9,2
ETFE-*g*-PSSA, DG: 36%	0.686 ±0.006	2.130 ±0.010	0.101 ±0.002	0.296 ±0.001	50.2	18.9	9.3
ETFE-*g*-PSSA, DG: 54%	0.624 ±0.004	2.119 ±0.030	0.083 ±0.001	0.295 ±0.002	50.5	18.3	10.1

Note that measured τ_i and I_i values are related to annihilations both in ETFE crystalline and amorphous domains and in grafted polystyrene phases for PS-grafted samples. Grafting reportedly occurs primarily in ETFE amorphous regions.[23,46] Moreover, our results (see DSC and DMA analyses below) revealed that grafting occurred in amorphous domains rather than crystalline regions. Inspection of τ_4 and R_4 values (Table 3) indicated a gradual decrease in nano-hole sizes in amorphous regions showing PS grafting. The expansion of PS-grafted regions in amorphous ETFE domains induces a certain compress ion in these domains. This shrinks the holes in these regions, leading to a gradual decrease in τ_4 and hence R_4 with increasing DG. The introduction of sulfonic acid groups in PS chains causes additional steric and electrostatic stress on amorphous ETFE domains, further shrinking the voids. Therefore, the comparison of τ_4 values between PS-grafted and sulfonated samples showing similar DG values reveals that the sulfonated membranes show smaller nano-holes. Moreover, the expansion of PS-grafted regions in amorphous ETFE domains appears to affect crystalline ETFE phases. The extremely low τ_3 of pristine ETFE increased significantly on PS grafting, leading to a nano hole radius of 0.126 nm at 17% (w/w) PS grafting. This indicates that the grafting-induced compression in amorphous regions induces some structural reorientations in densely packed crystalline domains, enhancing free-volume hole sizes in ETFE crystallites. However, the hole radius seems to change irregularly upon sulfonation rather than following DG.

Furthermore, the PAL spectrum provides information on the electronic structure of a material. Being the antiparticle of the electron, the positron exhibits similar properties to the electron except for its positive charge. This positively charged particle preferentially localises in regions of minimum positive charge density because of electrostatic repulsion. The PAL spectrum component intensities presented in Table 3 are related to the amount of positrons annihilated from free-state (I_2) and Ps-forming states in crystalline (I_3) and amorphous (I_4) domains. The relative intensity of free-state positron annihilations was higher for pristine ETFE than for PS-grafted films and I_2 gradually decreased with DG. A positron can be annihilated by one bound electron in a molecule to form a Ps. Bound electrons in ETFE are withdrawn by the fluorine atoms, which reduces electron availability for reaction with a positron and suppresses Ps formation[47]. The grafting of PS to ETFE supplies electron-donating phenyl groups to the composition, increasing the probability of Ps forming annihilations via combination with an electron. Therefore, PS grafted films exhibited lower I_2 values but higher I_3 and I_4 values compared to pristine ETFE and the intensities changed with DG. The sulfonation yields phenyl groups substituted with electron-withdrawing sulfonic acid functionalities. Therefore, Ps formation was inhibited in sulfonated membranes in agreement with previous studies,[44,48] reducing I_3 and I_4 and augmenting I_2 compared to PS-grafted films with similar DG values.

Thermal properties were evaluated by TGA, DSC and DMA. Thermal degradation profiles of organic and inorganic components were determined by TGA, whereas DSC provided insight on the thermal transition behaviour. The viscoelastic properties, such as dynamic mechanical behaviour, storage modulus (E'), loss modulus (E'') and $\tan\delta = E'/E''$ were obtained by DMA and used to study molecular mobility transitions such as the glass transition temperature, *Tg*. TGA, DSC and DMA results are summarized in Table 4.

Table 4. Thermal analysis results collected from TGA, DSC and DMA for pristine ETFE and graft-type ETFE samples.

Samples	TGA results				DSC results					DMA results	
	DG / wt %	T_{di} [a] /°C	T_{dm} [b] /°C	Residual mass / *wt %*	DG / wt %	T_m [c] /°C	ΔH_f / J g^{-1})	Cryst. / %	Corrected Cryst./%	DG / wt %	T_g / °C
Pristine ETFE			505.5	~0	-	265.6	36.51	32	32	-	107
PS-grafted Films	15	415	503.7	1.5	26	266.1	29.25	26	32.6	15	113
	26	410	503.1	1.2	40	265.7	24.55	22	31	36	122
	40	405	502.3	1.6	52	264.4	22.50	20	30	54	124
	52	400	503.1	1.3							
Sulfonated membranes	15	ND	509.5	10.2				15			121
	26	ND	509.4	14.0				36			~114
	54	ND	512.3	18.9				54			~113

[a]The initial thermal decomposition temperature (T_{di}) is the temperature, at which the decomposition rate indicates a significant weight loss d(wt %)/d*T*> 1% °C^{-1}). [b]The maximum decomposition temperature (T_{dm}) is the temperature, at which the highest decomposition rate is observed for the corresponding pattern. [c]melting temperature

Thermogravimetry (TG) curves of ETFE films and sulfonated membranes are shown in Fig. 5 for various grafting degrees. The derivative thermogravimetry (DTG) curves are provided in Fig. S14. The pristine ETFE film showed a simple thermal degradation curve, in which degradation occurred in one step starting at around 440 °C and reached a maximum rate at 504 °C. Moreover, PS presented a one-step degradation profile with initial (T_{di}) and maximum decomposition (T_{dm}) temperatures of 370 and 422 °C, respectively. However, the degradation profile of the PS-grafted films exhibited two distinct steps: one for the degradation of PS and another one for ETFE degradation. T_{di} values decreased with increasing DG for PS-grafted films, approaching those of pure PS (Table 4). Furthermore, the area of the first degradation step increased proportionally with the amount of PS grafted to ETFE, consistent with the gravimetrically calculated DG values. The initial weight loss observed in the thermograms of sulfonated membranes was ascribed to the loss of absorbed water from these strongly hydrophilic membranes. The amount of water absorbed changes proportionally with sulfonation as a consequence of DG. The elimination of sulfonic acid groups, accompanied by SO_2 gas emission, was observed at ca. 300°C.[49] This step was followed by the degradations of PS and ETFE domains at T_{dm} values of about 440 and 510 °C, respectively. TG and DTG curves showed that these degradation steps were difficult to discriminate from one another, but they appeared as a continuous weight loss between ca. 250 and 550 °C. Moreover, TGA related data demonstrate an increase in T_{dm} values during PS and ETFE degradation steps (Table 4), suggesting that the introduction of sulfonic acid groups enhances the heat resistance of the ETFE matrix. Moreover, the sulfonated membranes did not undergo complete degradation and some residues remained intact proportionally with DG (Fig. 5b and Table 4), indicating a thermal stability increase for the membranes at higher temperatures.

DSC thermograms of pristine ETFE, PS-grafted ETFE films and sulfonated membranes are shown in Figure S15. All thermograms present a strong endothermic transition at ca. 265 °C (Fig. S15a and Table 4), consistent with the melting of ETFE. The melting endotherms reached their maxima over a broader range at lower temperatures before returning to the baseline value, indicating differences in crystallite sizes. Crystallinity values calculated from the enthalpies of fusion decreased proportionally with DG. The incorporation of polystyrene grafts, which are amorphous in nature, increases the amorphous fraction of the entire film and thus reduces the crystalline proportion. This dilution of crystalline domains due to amorphous PS grafts has been reported in other previous studies.[50,51] To eliminate this effect and determine the inherent crystallinity of the ETFE substrate in grafted films, crystallinities were recalculated by subtracting the gravimetric contribution of grafted PS. The recalculated ETFE crystallinity in PS-grafted films was in a very good agreement with that of pristine ETFE (Table 4). Moreover, the comparison between peak maxima of PS-grafted films and that of pristine ETFE indicates little change in melting temperatures T_m. The agreement observed for T_m and recalculated ETFE crystallinity values reveal that grafting primarily occurs in amorphous ETFE domains. Slight changes in these values may be attributed to reorientations in crystalline ETFE domains because of the grafting-induced stress in amorphous regions, consistent with PALS results and previous studies.[51,52]

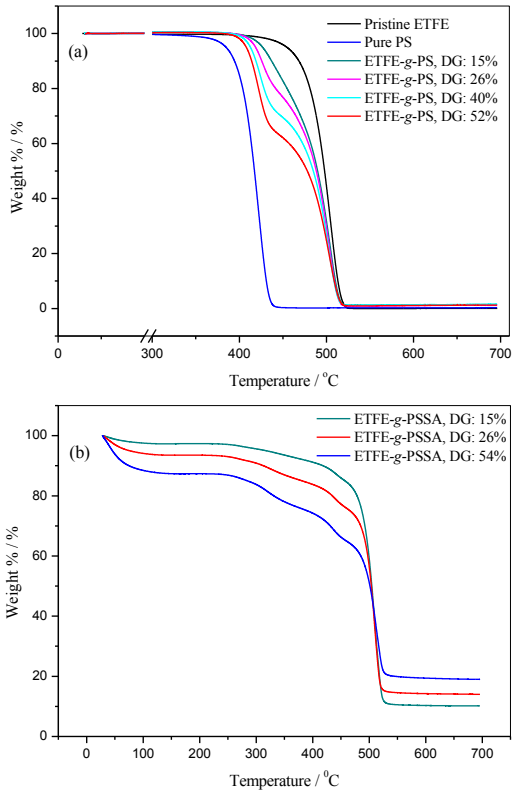

Fig. 5 Thermogravimetry curves of (a) pristine ETFE, pure PS and PS-grafted films with various degree of grafting (DG) and (b) sulfonated membranes with various DGs.

Sulfonated membranes showed broad endothermic peak ranging from ca. 50–180 °C, affecting the baseline up to 195°C (Fig. S15b). As discussed above, these peaks are attributed to the release of water molecules bound to sulfonic acid groups. Several drying procedures were investigated to minimise the interference of water on DSC measurements. Drying the sulfonated membranes at 100 °C for several days was found to diminish water absorption to some extent.[52,53] However, the membranes quickly absorbed water again and a clear water contribution was recorded because of non-removable or reabsorbed water (Fig. S15b). Alternatively, water may be removed by converting the acid form of the membrane to its salt form.[54] This conversion significantly changed the measured enthalpies of fusion and T_m values, offering an unpreferable process (Figure S16). Therefore, the membrane water content could not be reduced efficiently prior to DSC measurements, preventing crystallinity measurement for the membranes.

Having examined the crystalline domains, the microstructural changes occurring in the amorphous phases should also been considered. ETFE is a well-known semicrystalline polymer, having about 32% crystallinity as seen in Table 4. However, when ETFE is heated within a certain range of temperature below its decomposition temperature, the variations in heat capacity, corresponding to the change in specific volume near glass transition temperature (T_g), is probably too small to be detected by the DSC technique. Therefore, the T_g could not be ascertained from the DSC data. Only the PS-grafted sample with highest grafting degree yields a T_g at ca. 100 °C as can be seen in Figure S15a.

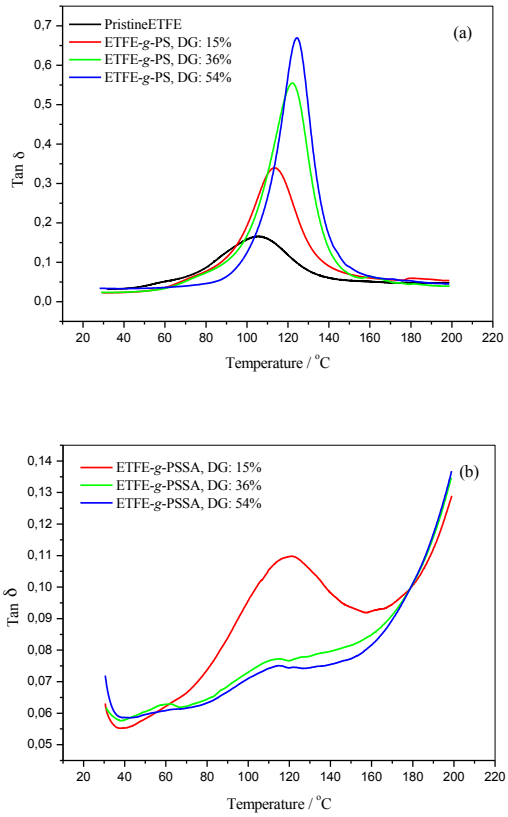

Fig. 6 Tanδ versus temperature curves of (a) pristine ETFE and PS-grafted films with various degree of grafting (DG) and (b) sulfonated membranes with various DGs.

To investigate the macromolecular mobility in amorphous phase, most of our effort was concentrated on a more sensitive method, i.e. the DMA technique. Fig. S17 shows the storage modulus (E') and loss modulus (E'') as a function of temperature for pristine and graft-type ETFE samples. Note that the storage modulus (elastic response) is related to stiffness, the loss modulus (viscous response) is related to energy dissipation and the E'/E'' ratio, which is also named as tanδ, is related to mechanical damping.[55] These three parameters vary significantly with temperature, especially around polymer relaxation phenomena such as glass transition. These changes in viscoelastic properties are strongly dependent on molecular motions and segmental mobility.[55] Thus, every factor affecting macromolecular mobility, such as crystallinity or small absorbed molecules, leads to significant changes of relaxation processes and viscoelastic properties of polymers.[56] The thermograms for damping tangent (tanδ = E'/E'') are presented in Fig. 6. The peak maxima of tanδ plots, yielding the T_g values are presented in Table 4. The T_g of pristine ETFE is observed at 107 °C, in agreement with previous works.[57,58] It is obvious from Figure 6a and Table 4 that incorporation of PS chains to ETFE substrate shifts the T_g to higher values because of covalent attachments in amorphous domains, inducing an increase in chain mobility restrictions. Sulfonation is expected to yield a further increase in T_g as it introduces strong hydrogen bonding interactions between different PS chains to restrict chain mobility in these domains.[59] However, in the case of sulfonation we encountered a decrease in T_g as a result of plasticization effects, which can be attributed to absorbed water, especially in membranes with high grafting degree. Attachment of water to polymer via hydrogen bonds may yield a plasticization effect as the inter- and intra-molecular hydrogen bonding along the polymer chains, provided by the sulfonic acid groups in our case, is intercepted by water molecules. This interaction strongly reduces interchain cohesion and mechanical integrity, and increases the fractional free volume of polymer, yielding a decrease in T_g.[60,61]

Note that the storage modulus of each sample does not provide any readable peaks as can be seen in Fig. S17a and S17c. Nevertheless, significant changes indicating a progressive loss at the elastic property of the samples are observed over the temperature range. This further indicates that grafting of PS and subsequent sulfonation significantly increases the storage modulus. The gradual slight increase of storage modulus, which indicates a plasticizing effect, observed for sulfonated membranes up to ca. 100 °C is attributed to removal of residual water.[56] Loss modulus (E'') plots of samples show some peaks as can be seen in Figures S17b and S17d. In principle, both E'' and tanδ can be used to measure the characteristic temperatures matched with various relaxation processes. Loss modulus plots indicate similar observations with those achieved by tanδ plots with some quantitative differences as has previously been reported.[62,63]

Investigation of membrane properties

Membrane properties, including proton conductivity and their comparisons, with those from other studies and commercial samples are presented in Table 5. The conductivity values for radiation-induced grafted membranes reported in the literature vary over a wide range. The comparison of our PEMs with commercial Nafions and PEMs prepared in similar systems, in which the same substrate (i.e. ETFE) was used but PS-grafting was performed via conventional method rather than RAFT, reveals significant enhancements in proton conductivities associated with RAFT method. Among the PEMs utilizing ATRP or NMP methods[7-9], PEMs by Zhai et al.[8] present quite high proton conductivity values (e.g. 200 mScm^{-1} at ~50 % graft ratio). However, they applied γ-initiated grafting of 2-bromotetrafluoroethyl trifluorovinyl ether (BrTFF) via the conventional method to achieve bromine-containing grafts that are essential for ATRP. Then, the bromine atoms in the poly(BrTFF) grafts grown in an uncontrolled manner were used as initiators in the ATRP of styrene. Therefore, we believe that considering the whole grafting as a controlled process is not correct.

Fig. 7 shows the evaluation of experimental and theoretical ion exchange capacity (IEC) versus degree of grafting (DG). There is a good agreement between theoretical and experimental ion exchange capacities at low DGs. However, the measured ion exchange capacities are lower than the calculated ones at higher DG values. With increasing graft ratio, sterical effects become more prominent which may result in suppression of the sulfonation reactions. Besides, two sulfonic acid groups may combine and form a sulfone bond at high temperatures during membrane preparation, which causes incomplete ion exchange with NaCl.[46] The ratio between theoretical and experimental IEC values gives the degree of sulfonation (DS). DS changes in the range of ca. 85-95 % depending on the DG value. The IEC values attained in this study exceed that of the Nafion membrane for all DG values as can be seen in Table 5, indicating a sufficient sulfonation.

Table 5. Membrane properties achieved in this study and their comparisons.

PS graft ratio, DG / %	Conductivity / $mScm^{-1}$	IEC / ($meqg^{-1}$)	water uptake / %	hydration number; nH_2O/nSO_3H
14[a]	3.4	1.06	12	10
24[a]	14	1.24	27	12.5
37[a]	42.8	1.65	41	13,1
48[a]	148.5	2.03	64	17
45[b]	~70	na[c]	45	11
51.7[d]	41	2.22	14.2	3.55
40[e]	80	1.73	55	18
38[f]	17	2.3	42	10
50[f]	25	2.2	36	9
~50[g]	200	~2.2	~75	~19
Nafion 105[h]	56	1.00	51	28
Nafion 117[h]	51	0.89	37	23

[a] membranes in this study by RAFT-mediated grafting; [b] ETFE-based PEM by conventional method, ref.64; [c] not available; [d] ETFE-based PEM by conventional method and cross-linking, ref.65; [e] PVDF-based PEM by NMP, ref. 9; [f] PVDF-based PEM by ATRP, ref. 7; [g] ETFE-based PEM by ATRP, ref. 8; [h] commercial Nafion 105 and 117, ref. 66

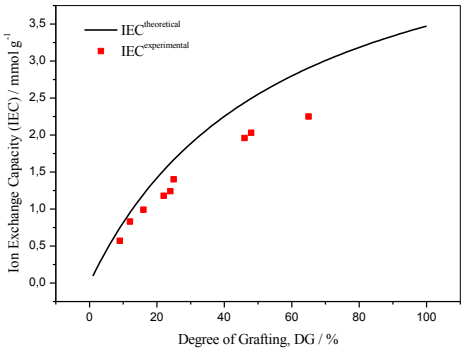

Fig. 7 Evaluation of experimental and theoretical ion exchange capacity (IEC) versus degree of grafting (DG).

Conclusions

Novel promising ETFE-based membranes for fuel cell applications have been synthesized using RAFT polymerization. The introduction of RAFT polymerization enhanced the structural uniformity and presented a promising increase in terms of proton conductivity compared to conventional method. We believe that the use of RAFT in RIG technique opens the door to designing new tuneable membranes in a controlled manner by a one-step method under mild conditions. We hope that this model work provides new initiatives for the design of PEMs with enhanced properties to replace DuPont's Nafion perfluorosulfonic acid membranes and helps in the future development of fuel cells.

Acknowledgments

The authors thank Dr. Günther G. Scherer and Dr. Celestino Padeste from the Paul Scherrer Institute, PSI, Switzerland for supplying the ETFE films and for the help in preparation of hot-pressed ETFE films, respectively.

Notes and References

1 V. Mehta, J. S. Coopeer, *J. Power Sources,* 2003, **114**, 32–53.
2 F. Bruijn, *Green Chem*., 2005, **7**, 132–150.
3 Y. Shao, G. Yin, Z. Wang, Y. Gao, *J. Power Sources,* 2007, **167**, 235–242.
4 K. A. Mauritz, R. B. Moore, *Chem. Rev.,* 2004, **104**, 4535−4585.
5 S. A. Gürsel, L. Gubler, B. Gupta, G.G. Scherer, *Adv. Polym. Sci.,* 2008, **215**, 157–217.
6 W. A. Braunecker, K. Matyjaszewski, *Prog. Polym. Sci.,*2007, **32**, 93–146.
7 S. Holmberg, P. Holmlund, C.-E. Wilen, T. Kallio, G. Sundholm, F. Sundholm, *J. Polym. Sci. Pol. Chem.,* 2002, **40**, 591–600.
8 M. Zhai, J. Chen, S. Hasegawa, Y. Maekawa, *Polymer,* 2009, **50**, 1159–1165.
9 S. Holmberg, P. Holmlund, R. Nicolas, C.-E. Wilen, T. Kallio, G. Sundholm, F. Sundholm, *Macromolecules,* 2004, **37**, 9909–9915.
10 M. Semsarilar, S. Perrier, *Nature Chemistry,* 2010, **2**, 811–820.
11 M. Barsbay, O. Güven, H. Bessbousse, T. L. Wade, F. Beuneu, M.-C. Clochard, *J. Membr. Sci.,* 2013, **445**, 135-145.
12 M.-M. Titirici, B. Sellergren, *Chem. Mater.,* 2006, **18**, 1773–1779.
13 M. Barsbay, O. Güven, M. H. Stenzel, T. P. Davis, C. Barner-Kowollik, L. Barner, *Macromolecules,* 2007, **40**, 7140–7147.
14 M. Barsbay, O. Güven, T. P. Davis, C. Barner-Kowollik, L. Barner, *Polymer,* 2009, **50**, 973–982.
15 M. Barsbay, O. Güven, *Radiat. Phys. Chem.,* 2009, **78**, 1054–1059.
16 C. Barner-Kowollik, J. F. Quinn, T. L. U. Nguyen, J. P. A. Heuts, T. P. Davis, *Macromolecules,* 2001, **34**, 7849−7857.
17 N. Djourelov, Z. Ates, O. Güven, M. Misheva, T. Suzuki, *Polymer,* 2007, **48**, 2692-2699.
18 G. Moad, In *Controlled Radical Polymerization: Mechanisms*, 1st ed.; K. Matyjaszewski, B. S. Sumerlin, N. V. Tsarevsky, J. Chiefari, Eds.; *ACS Symposium Series*, 2015,**1187**, 211.
19 M. Barsbay, O. Güven, *Polymer,* 2013, **54**, 4838-4848.
20 Y. Kodama, M. Barsbay, O. Güven, *Radiat. Phys. Chem.,* 2014, **105**, 31-38.
21 H.-P. Brack, H.G. Bührer, L. Bonorand, G. G. Scherer, *J. Mater Chem.*, 2000, **10**, 1795-1803.
22 M. M. Nasef, E. S. Hegazy, *Prog. Polym. Sci*., 2004, **29**, 499–561.
23 B. Gupta, G. G. Scherer, *Angew. Makromol. Chem.*, 1993, **210** (3655), 151.

24 G. Moad, J. Chiefari, R. T. A. Mayadunne, C. L. Moad, A. Postma, E. Rizzardo, S. H. Thang, *Macromol. Symp.*, 2002, **182**, 65–80.

25 E. Jabbari , N. A. Peppas, *Macromolecules*, 1993, **26 (9)**, 2175–2186

26 J. Jang, K. Lee , *Chem. Commun*., 2002, **10**, 1098-1099.

27 A. Mokrini, J. L. Acosta, *Polymer*, 2001, **42**, 9-15.

28 S. Zhaohui, S. L. Hsu, X. Li, *Macromolecules*, 1994, **27**, 287–291.

29 G. Zundel, *Hydration and intermolecular interaction*; Academic Press: New York, 1969.

30 A. Sangyun, S.A. Lee, S. H. Sang Hyup Oh, W. Lee, *J Colloid Interface Sci.,* 2009, **332**, 461–466.

31 E. Ploetz, S. Laimgruber, S. Berner, W. Zinth, P. Gilch, *Appl. Phys. B,* 2007, **87**, 389–393

32 B. Schrader, *Infrared and Raman Spectroscopy*, VCH, Weinheim, 1995, 187.

33 S. Radice, N. Del Fanti, C. Castiglioni, M. Del Zoppo, G. Zerbi, *Macromolecules*, 1994, **27**, 2194-2199.

34 A. Jayakumar, S. P. Sethu, M. Ramos, J. Robertson, A. Al-Jumaily, *Ionics*, 2015, **21**, 1-18

35 A. B. LaConti, M. Hamdan, R. C. McDonald, In *Handbook of Fuel Cells—Fundamentals, Technology and Applications*, Wiley, New York, NY, 2003, *3*, 647.

36 K. Haraya, S. T. Hwang, *J. Membr. Sci.,* 1992, **71**, 13-27.

37 D. W. Gidley, H.-G. Peng, R. S. Vallery, *Annual Reviews in Material Research*, 2006, **36**, 349

38 V. P. Shantarovich, *Journal of Nuclear and Radiochemical Sciences*, 2001, **2**, R23-R26

39 J. Schultz, K. G. Lynn, *Rev. Mod. Phys.,* 1988, **60**, 701-779.

40 M. J. Puska, R. M. Nieminen, *Rev. Mod. Phys.,* 1994, **66**, 841-897.

41 A. P. Mills, *Science,* 1982, **218**, 335-340.

42 S. J. Tao, *J. Chem. Phys*., 1972, **56**, 5499

43 M. Eldrup, D. Lightbody, J. N. Sherwood, *Chem. Phys*., 1981, **63**, 51.

44 S. Sawada, A. Yabuuchi, M. Maekawa, A. Kawasuso, Y. Maekawa, *Radiation Physics and Chemistry* , 2013, **87**, 46–52

45 H. F. M. Mohamed, E. E. Abdel-Hady, S. S. Mohamed, *Radiat. Phys. Chem*., 2007, **76**, 160.

46 J. Chen, M. Asano, T. Yamaki, M. Yoshida, *Journal of Membrane Science,* 2006, **269**, 194–204.

47 D. Bamford, G. Dlubek, G. Dommet, S. Horing, T. Tupke, D. Kilburn, M. A. Alam, *Polymer*, 2006, **47**, 3486-3493.

48 Y. Kobayashi, H. F. M. Mohamed, A. Ohira, *Journal of Physical Chemistry B*, 2009, **113**, 5698-5701.

49 M. M. Nasef, H. Saidi, *Polymer Degradation and Stability,* 2000, **70**, 497-504.

50 M. M. Nasef , *European Polymer Journal* , 2002, **38**, 87-95

51 S. Hietala, M. Paronen, S. Holmberg, J. Näsman, J. Juhanoja, M. Karjalainen, R. Serimaa, M. Toivola, T. Lehtinen, K. Parovuori, G. Sundholm, H. Ericson, B. Mattsson, L. Torell, F. Sundholm, *Journal of Polymer Science Part A: Polymer Chemistry*, 1999, **37**, 1741–1753.

52 M. M. Nasef, H. Saidi, H. M. Nor, OM Foo, *J.Appl. Polym. Sci*., 2000, **78**, 2443–2453.

53 M. M. Nasef, H. Saidi, *Macromol. Mater. Eng.,* 2006, **291**, 972.

54 S. A. Gürsel, J. Schneider, H. B. Youcef, A. Wokaun, G. G. Scherer, *Journal of Applied Polymer Science*, ***2008***, **108**, 3577–3585.

55 J. D. Ferry, *Viscoelastic properties of polymers,* Wiley, New York, 1980.

56 E. Sgreccia, J.-F. Chailan, M. Khadhraoui, M. L. Di Vona, P. Knauth, *Journal of Power Sources,* 2010, **195**, 7770–7775

57 V. Saarinen, M. Karesoja, T. Kallio, M. Paronen, K. Kontturi, *J. Membr. Sci*., 2006, **280**, 20-28.

58 J. Feng, C.-M. Chan, *Polymer*, 1997, **38**, 6371–6378.

59 K. A. Mauritz, R. I. Blackwell, F. L. Beyer, *Polymer*, 2004, **45**, 3001–3016.

60 J. M. Lagaron, A. K. Powell, G. Bonner, *Polymer Testing,* 2001, **20**, 569–577.

61 T. Watari, H. Wang, K. Kuwahara, K. Tanaka, H. Kita, K. Okamoto, *J. Membr. Sci.,* 2003, **219**, 137–147.

62 A. Genovese, R. A. Shanks, *Macromol. Mater. Eng*., 2004, **289**, 20.

63 K. P. Menard, *Dynamic Mechanical Analysis: A Practical Introduction*; CRC Press: Boca Raton, 1999.

64 Y. Kimura, M. Asano, J. Chen, Y. Maekawa, R. Katakai, M. Yoshida, *Radiat.Phys. Chem.,* 2008, **77**, 864–870.

65 L. Gubler, N. Prost, S. A. Gürsel, *Solid State Ionics*, 2005, **176**, 2849–2860.

66 T. Kallio, M. Lundström, G. Sundholm, N. Walsby, F. Sundholm, *J. Appl.Electrochem.,* 2002, **32(1),** 11-18

"for Table of Contents use only"

Towards New Proton Exchange Membrane Materials with Enhanced Performance via RAFT Polymerization

Gökçe Çelik, Murat Barsbay, Olgun Güven*